Title	Modeling tendon-sheath mechanism with flexible configurations for robot control
Author(s)	Wang, Zheng; Sun, Zhenglong; Phee, Soo Jay
Citation	Wang, Z., Sun, Z., & Phee, S. J. (2013). Modeling tendon -sheath mechanism with flexible configurations for robot control. Robotica, 31(7), 1131-1142.
Date	2013
URL	http://hdl.handle.net/10220/18669
Rights	

Robotica (2013) volume 31, pp. 1131–1142. © Cambridge University Press 2013
doi:10.1017/S0263574713000386

Modeling tendon-sheath mechanism with flexible configurations for robot control

Zheng Wang†, Zhenglong Sun‡* and Soo Jay Phee‡

†*Wyss Institute for Biologically Inspired Engineering, Harvard University, Cambridge, MA, USA*
‡*School of Mechanical and Aerospace Engineering, Nanyang Technological University, Singapore*

(Accepted April 11, 2013. First published online: May 14, 2013)

SUMMARY
Surgical and search/rescue robots often work in environments with very strict spatial constraints. The tendon-sheath mechanism is a promising candidate for driving such systems, allowing power sources and actuation motors placed outside to transmit force and energy to the robot at the distal end through the constrained environment. Having both compactness and high force capability makes it very attractive for manipulation devices. On the other hand, the friction attenuation of tendon tension is nonlinear and configuration-dependent due to tendon/sheath interactions throughout the transmission path. This is a major obstacle for the tendon-sheath mechanism to be widely adopted. Here, we focus on the friction analysis for flexible and time-varying tendon-sheath configurations: the most challenging but yet commonly encountered case for real-world applications. Existing results on fixed-path configurations are reviewed, revisited, and extended to flexible and time-varying cases. The effect of tendon length to friction attenuation is modeled. While focusing on tension transmission, tendon elongation is also discussed with the length effect applied. In the end, two-dimensional results are extended to three-dimensional tendon-sheath configurations. All propositions and theorems are validated on a dedicated experimental platform.

KEYWORDS: Control of robotic systems; Force control; Surgical robots; Haptic interfaces; Teleoperation.

1. Introduction

Robots are often designed to work in highly space-constrained environments difficult or inaccessible for human beings. For instance, the gaps of a rescue site,[1] the interconnected pipes of a sewer system,[2] or the winding tunnels of a human body.[3,4] An ideal solution to the spatial constraint would be self-contained miniature wireless robots. However, with the restricted size and energy supply,[5] the functionalities of such miniature robots are primitive. To enable efficacious physical intervention with the environment, the relatively high mechanical power required to drive the robot needs to be supplied from outside, where size is not a constraining factor. This, however, requires transmitting mechanical power from the outside actuator to the distal robot manipulator through a long and thin neck (such named to differentiate from the robotic arms on the distal end of the robot) that can pass along the complex environment.

Several mechanisms are found viable for such applications. Cable-pulley mechanism is the simplest in redirecting force transmission, but a predefined route is required for pulley installation.[6] Continuum/hyper-redundant mechanism is able to bend to bypass obstacles and transmit the mechanical power to the distal end.[7,8] However, the actuation of distal segments often influences the shape of proximal segments, resulting in low payload if passing through a long and winding route.[9] Another promising solution is the tendon-sheath mechanism. Originated from human anatomy, the tendon-sheath mechanism transmits power by pulling a tendon surrounded by an outside supporting sheath, where the tendon is used to pull and control the motion of a joint, the sheath is used as a cover to encase and protect the tendon, while guiding the pulling direction. The relative motion between tendon and sheath allows tension to be transmitted from the proximal end to the distal end, even through a route with arbitrary curvatures. The tendon-sheath system (TSS in short) will be the focus throughout this paper.

Prone to friction loss is a main disadvantage for the TSS. Since the sheath encircles the tendon throughout the length of the TSS, friction between the two is configuration-dependent, hence is nonlinear and affected by the characteristics of the TSS. In common applications such as rescue/surgical robotics, placing sensors at the distal end is often not possible due to strict space limitations.[10] It is only possible to place the position and force sensors at the proximal end near the actuation before the transmission mechanism. Therefore, without sensory feedback at the distal end, in the applications that adopting TSS as actuation, the control performance would be solely depending on an open-loop controller. Since the driving source and the robot are at two different ends of the TSS, by proposing a generic transmission model of the flexible TSS, we could determine the friction loss on the transmission route, hence calculate the force at the distal end by measuring the force at the proximal end.

The TSS as a mechanism has been well studied. Lee and Tsai[11] discussed the kinematic structures of tendon-driven robotic arms in order to identify and enumerate them. Kobayashi *et al.*[12] discussed the controllability of the TSS with redundant tendon. Focusing on the power transmission, Kaneko *et al.*[13] introduced a tendon-sheath model to formulate the force and elongation transmission

* Corresponding author. E-mail: sunz0006@e.ntu.edu.sg

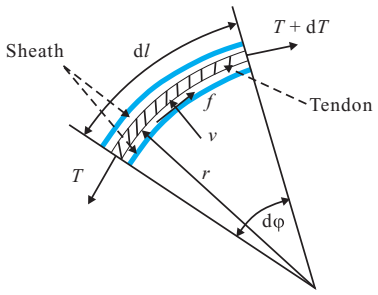

T	Tension of the tendon
δ	Elongation of the tendon
$\rho = \frac{1}{EA}$	Tendon property
ζ	Direction index
ξ	Displacement of the tendon
ν	Normal force
f	Friction force
μ	Friction coefficient
r	Radius
κ	Curvature
φ	Curve angle
l	Tendon length

Fig. 1. (Colour online) A small segment of a tendon-sheath system.

characteristics. Palli and Melchiorri,[14] Tian and Wang,[15] and Chen *et al.*[16] adopted different dynamic friction models into the tendon-sheath transmission model. Agrawal *et al.*[17] discussed transmission characteristics of the TSS in a closed-loop configuration. Existing works focus on power transmission of the TSS with fixed radius configurations in a plane. However, the new challenge is the flexibility requirement posed by the complex environment: in order to maneuver among a narrow space, the robot with its TSS neck must be able to change configuration from time to time. In case of the robotic devices operated by a human operator, previous studies measuring human haptic behaviors[18–20] suggest that the human haptic operation is not deterministic, hence it is not applicable to predefine the operation routes and assume the transmission path to be fixed during haptic operations by human operators. This calls for flexible TSS of time-varying configurations. There have been pioneering research works along this direction, Low *et al.*[21] and Phee *et al.*[22] analyzed the TSS with random curvature combinations, and proposed a remedy to characterize the model coefficients once the configuration changed.

In this paper, we will discuss in depth the friction problem of the TSS under flexible time-varying conditions, in two-dimensional (2D) planes as well as three-dimensional (3D) spaces. We will prove theoretically for a concise formula for 2D, and also prove that it is not applicable to 3D, while proposing 3D solutions. We also argue that length has a penalty effect on tension transmission and give estimations. Elongation is discussed toward the end. All propositions are validated by experimental results.

2. Transmission Characteristics of TSS

2.1. Problem definition and terminology

Consider a small segment of tendon and sheath in a 2D plane. The related variables, constants, and their directions are shown in Fig. 1. Here, T and δ are the tension and the elongation of the tendon, respectively. ρ is a property of the tendon defined by the inverse of Young's modulus E multiplied by the cross-sectional area A, taken as constant for a given tendon. ζ is the direction index, where in case of sliding $\zeta = \mathrm{sgn}\dot{\xi}$, ξ being the displacement of the entire tendon in the sliding case. σ is the compression force of the sheath. ν is the normal force applied to the tendon by the sheath, resulting in the friction force f, with the friction coefficient μ. r and κ are the radius and the curvature of the current tendon segment, respectively, with $\mathrm{d}\varphi$ the curve angle, and $\mathrm{d}l$ the length of the tendon segment. Given the infinitesimal segment, the tendon and the sheath are considered to have the same length $\mathrm{d}l$.

From Fig. 1, the basic relations of the variables can be written as follows:

$$r = 1/\kappa,\ \mathrm{d}l = r\mathrm{d}\varphi,\ f = \nu\mu,\ \nu \cong T\mathrm{d}\varphi,\ \mathrm{d}T = -f\zeta. \quad (1)$$

Hence, the change of tendon tension on the segment in study, caused by tendon-sheath friction, can be derived from the basic equations in Eq. (1) as:

$$\frac{\mathrm{d}T}{\mathrm{d}l} = -\frac{\mu}{r}T\zeta. \quad (2)$$

Till now, the discussions are about the infinitesimal segment of the TSS. From Eq. (2), it follows naturally that, by integrating the tension changes over the entire length of the tendon, we can obtain the tension transmission at the distal end of the tendon

$$T_L = -\int_0^L \frac{\mu\zeta}{r(l)}T(l)\,\mathrm{d}l + T_{in} + T_0, \quad (3)$$

where L is the total length of the tendon, T_{in} is the tension applied to the beginning of the tendon, T_L is the tension transmitted to the end of the tendon, and T_0 is pretension. Note here, both T and r are functions of l.

The actual function of $r(l)$ is required to calculate the transmission function (3) analytically. When the TSS is flexible, $r(l)$ would be either not known priorly, or not measurable at all. A remedy has been proposed previously by Phee *et al.*.[22] Phee *et al.* proposed an approach to precalibrate the function to access the coefficients of the transmission function. They argued that for their application, the changes to the configuration, and hence $r(l)$, would be negligible after calibration. This approach applies ideally for the TSS with unknown but fixed-path configurations, for instance, the robot neck gets fixed once reached the targeted area, while

only the distal end robotic arms operate. But for generic and possibly time-varying configurations, it is not feasible to calibrate the transmission function adaptively. Therefore, a new approach is needed to address this problem.

Several assumptions regarding the TSS and their working conditions are listed below, prior to detailed discussion, followed by necessary remarks.

Assumption 1. The loss of tension on the tendon is solely caused by friction between the tendon and the sheath.

Assumption 2. The external load change is sufficiently slow, such that any tension change can be sufficiently transmitted along the tendon, and the tendon slides inside the sheath in one direction.

Assumption 3. Both the tendon and the sheath are uniform, such that ρ and μ are constant.

Assumption 4. The elongation of the tendon can only be positive. The sheath does not change in length.

Assumptions 1 and 2 are generally accepted. They have already been considered in Eqs. (1) and (2). It can be derived from Assumption 2 that ζ is constant. Assumption 3 is about the uniformity of the tendon and the sheath. Assumption 4 suggests that $\delta \geq 0$, since the tendon will get loose instead of being compressed.

2.2. *Transmission in 2D configuration with constant radius*

Existing works generally consider applications with configurations in 2D planes with constant radii.[13–16] This is a valid assumption for certain applications like robotic hand actuation:[23] the TSS either encircles a supporting mechanism around a turning point with a constant radius, or follows a straight line between two turning points. Between turning points, friction is generally ignored in existing studies.

Here, the results of tension transmission and elongation of the TSS in 2D with constant radius are listed first.

If the curve radius is constant, denoted by R to separate from the general radius r, it becomes independent of the tendon length l. Therefore, it can be taken out from the integral of Eq. (3), resulting in the simple form of tension transmission

$$T_l = \begin{cases} T_{in} e^{-\frac{\mu l \zeta}{R}}, & \text{if } l < L_1, \\ T_0, & \text{if } l \geq L_1. \end{cases} \tag{4}$$

Here, the term L_1, as introduced by Kaneko *et al.*,[13] stands for the maximum length along the tendon until where the input tension can be transmitted. If $L_1 < L$, then the input tension cannot be efficiently transmitted to the end of the tendon, such that $T_l = T_0$ for all $L_1 < l < L$.

Similarly to tendon tension, the elongation δ of the tendon under input tension T_{in} is as follows:

$$\delta_l = \begin{cases} \dfrac{\rho R}{\mu} T_{in} \zeta \left(1 - e^{-\frac{\mu \zeta l}{R}}\right) - \rho T_0 l, & \text{if } l < L_1, \\ \dfrac{\rho R}{\mu} T_{in} \zeta \left(1 - e^{-\frac{\mu \zeta L_1}{R}}\right) - \rho T_0 L_1, & \text{if } l \geq L_1. \end{cases} \tag{5}$$

Although Eq. (4) is short and concise, it is only applicable for TSS with constant and time-invariant radii. For our discussion, the consideration differs in two major aspects: (1) with the sheath always encircling the tendon, length of the overall TSS may affect transmission characteristics, even in straight lines; and (2) relaxation of the fixed/constant radius requirement. We shall address both issues in the remainder of this section.

2.3. *The TSS length effect*

In existing studies, a generally accepted assumption is that friction is only caused by bending. Recall Eq. (1), the friction force f is a sole function of the normal force v. Hence, tension loss would only happen at corners; no tension loss for straight lines of any length. Different from cable/pulley systems, for the TSS the sheath encircles the tendon even at straight lines. Depending on the relative diameters of the two, surface contact could result in tension changes throughout the entire length of the TSS. Coincide with the common sense that the longer the transmission, the more significant the transmission loss, we observed length-related differences in our pilot experiments. Hence, a proposition is formulated below, which is further verified by validation experiments presented later in Section 3.3.

Proposition 1 (Length penalty). *The length of the TSS has an effect on tension transmission that can be approximated by a linear relationship between length and tension loss as follows:*

$$\mathrm{d}\tilde{T} = -\alpha \cdot \mathrm{d}l. \tag{6}$$

Here, α is a parameter representing the per-unit-length tension change due to the nonbending interaction between tendon and sheath. The minus sign is introduced to make α a positive value. For the scope of this study, we assume that α is constant for a given pair of tendon and sheath, such that the length penalty of each pair is linear and can be calibrated priorly. Later validation results will support this in Section 3.

2.4. *Tension transmission model for flexible TSS in 2D*

A length-dependent term was introduced to the friction force in Proposition 1 to address the effect of length to tension transmission. In this section, we will discuss tension transmission for flexible TSS.

The main argumentation of the new model is that, since for flexible TSS the radius of each segment of the tendon is a time-varying term that is difficult, if not impossible, to measure, radius should be removed from the expression of tendon transformation. Instead, an easier-to-measure quantity should be used to replace radius, which would make real-time tendon tension calculation possible for flexible TSS.

Combining Eqs. (1) and (6),

$$\mathrm{d}T = (-f + \mathrm{d}\tilde{T})\zeta = -\frac{\mu}{r} T \zeta \, \mathrm{d}l - \alpha \zeta \, \mathrm{d}l, \tag{7}$$

hence Eq. (3) is rewritten due to the new dT as

$$T_L = -\int_0^L \frac{\mu\zeta}{r(l)} T(l)\,\mathrm{d}l - \int_0^L \alpha\zeta\,\mathrm{d}l + T_{in} + T_0, \quad (8)$$

and consider Eq. (1), $\mathrm{d}l = r \cdot \mathrm{d}\varphi$, hence

$$T_\Phi = -\int_0^\Phi \mu\ \zeta\ T(\varphi)\,\mathrm{d}\varphi - \alpha L\zeta + T_{in} + T_0. \quad (9)$$

Here, the curve angle Φ is calculated as the sum of all the convexing curve angles along the TSS

$$\Phi = \int_0^{\varphi_L} |\mathrm{d}\varphi| = \sum_{i=1}^{n} |\Phi_i|, \quad (10)$$

where n denotes the number of convex segments throughout the length, Φ_i is the curve angle of each convex segment. In the integral form, φ_L denotes the curve angle at length L. In other words, Φ is the integration of the absolute value of each infinitesimal curve angle.

The accumulated curve angle Φ is simply the algebraic angle difference between the start and the end of the TSS, if the entire configuration remains convex; but if the configuration is nonconvex, then Φ is the sum of the absolute value of the curve angle of each convex segment (see more discussion on Φ in Section 3).

From Eq. (9), μ and ζ are both independent of φ. The curvature/radius term has been removed from the expression by changing the integral variable. Then, the integral over φ can be calculated as

$$T_\varphi = \begin{cases} T_{in}e^{-\mu\bar{\varphi}\zeta} - \alpha L\zeta, & \text{if } \varphi < \Phi_0, \\ T_0, & \text{if } \varphi \geq \Phi_0, \end{cases} \quad (11)$$

where Φ_0, similar with L_1 in Eq. (5), is a function of input tension T_{in} determined as follows:

$$\Phi_0 = \min\{\varphi \mid T(\varphi) = T_0\}. \quad (12)$$

Equations (11) and (12) describe the tension transmission of the TSS without putting constraints on the curvature/radius. From Eq. (11), the variable to determine the tension transmission is solely the accumulated curve angle of the entire tendon length.

An interesting remark following Eq. (11) is: as long as the accumulated curve angle does not change, reconfiguration of the TSS does not affect tension transmission. This is particularly important for flexible TSS applications: since only the *accumulated curve angle* but not the *exact configuration* is required to be the same, it allows for changing the configuration while maintaining the accumulated curve angle, and tension transmission would not be affected, hence the TSS can be truly *flexible*. Demonstration experiments are carried out to assess this property in Section 3.

2.5. An elongation model for flexible TSS in 2D

The elongation of TSS is the extended length of the tendon resulting from the applied tension. It is important to obtain accurate information of tendon elongation to achieve fine position control. However, elongation is a highly nonlinear time-varying function of the input tension. Similar to the discussion on tension transmission, the existing models in tendon elongation are also based on the assumption of constant radius/curvature throughout the TSS. Here, the discussion is extended to the effect of length and flexible TSS regarding elongation.

Recall the basic relations in Eq. (1) and the discussion on elongation in constant radius case in Eq. (5). With pretension T_0, we have

$$\frac{\mathrm{d}\delta(\varphi)}{\mathrm{d}\varphi} = r\rho(T(\varphi) - T_0) = r\rho T_{in}e^{-\mu\varphi\zeta} - r\rho\alpha l\zeta - r\rho T_0. \quad (13)$$

Integrate on both sides of Eq. (13), with $\delta(0)$=0, ρ, T_{in}, and T_0 constant, we get

$$\delta(\varphi) = \rho T_{in}\int_0^\varphi re^{-\mu\zeta\varphi}\,\mathrm{d}\varphi - \rho\alpha\zeta\frac{l_\varphi^2}{2} - \rho T_0 l_\varphi, \quad (14)$$

where φ and l_φ are the matching curve angle and curve length from the starting of the tendon to the current point of study.

Unfortunately, unlike tension transmission, because of the term r in Eq. (14), which is a time-varying function of φ, the integral cannot be solved analytically unless the exact function of $r(\varphi)$ is known. Hence, besides adding the length penalty effect, changing the integration variable from length l to curve angle φ does not make as significant a change in elongation as in tension transmission: configuration of the TSS still affects elongation calculation. Application-oriented remedies could be developed to minimize or eliminate the effect, such as by Phee *et al.*'s work,[22] but they are beyond the scope of this paper and are hence not included here.

Combining the discussions on tension transmission and elongation, we now propose a theorem for the model of flexible TSS.

Theorem 1 (2D). *For a TSS in 2D with terms as defined in Eq. (1) and input tension of T_{in}, the tension and elongation at each point along the TSS are given by Eqs. (11) and (14), respectively.*

Theorem 1 relaxes the constant radius constraint for 2D TSS, founding a basis for flexible TSS analysis. It also takes into account the length penalty effect proposed earlier, which would help addressing the length-related tension losses when they cannot be neglected. For tension transmission, Theorem 1 allows for total flexibility, as long as the TSS is kept convex and the accumulated curve angle is maintained; for elongation, Theorem 1 shows that flexibility will affect elongation, hence other measures must be considered for precise position control.

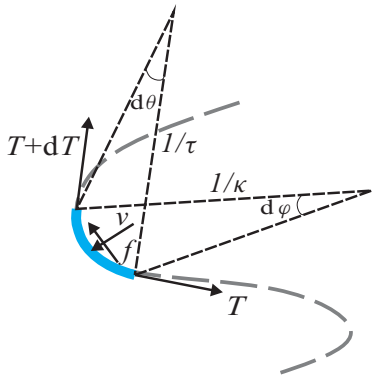

T	Tension of the tendon
δ	Elongation of the tendon
$\rho = \frac{1}{EA}$	Tendon property
ν	Normal force
f	Friction force
μ	Friction coefficient
κ	Curvature
τ	Torsion
φ	Curvature angle
θ	Torsion angle
l	Tendon length

Fig. 2. (Colour online) A small segment of a tendon-sheath system in 3D.

2.6. Tension transmission model for flexible TSS in 3D

So far the discussion has been limited to 2D configurations, similar with most of the literature. However, for real-world applications, it is inevitable to configure the TSS in 3D space. To the best knowledge of the authors, no studies have been published on 3D TSS analysis.

For a curve in 3D space, the very first challenge is that the curvature as defined in 2D is no longer sufficient in describing the configuration of the curve. Therefore, we need to go back to the modeling of an infinitesimal segment of the TSS to start the discussion in 3D.

An illustration of an infinitesimal 3D TSS segment is shown in Fig. 2. In addition to the terminologies in Fig. 1, here we introduce the torsion τ and the following relations for 3D flexible TSS:

$$\mathrm{d}\theta = \tau \cdot \mathrm{d}l. \tag{15}$$

The definition of curvature and torsion follows the convention of the Frenet–Serret system. Since the normal and binormal vectors are always orthogonal, the normal forces of both directions are also orthogonal to each other. Moreover, the resulting friction forces are both along the tangential vector. Therefore, we can calculate the algebraic summation of the friction force f is as follows:

$$f = \mu\nu \cong \mu\sqrt{(T\mathrm{d}\varphi)^2 + (T\mathrm{d}\theta)^2}. \tag{16}$$

Therefore, considering Eqs. (15) and (1):

$$\mathrm{d}T \cong -T\mu\zeta\sqrt{(\mathrm{d}\varphi)^2 + (\mathrm{d}\theta)^2} = -T\mu\zeta\sqrt{\kappa^2 + \tau^2}\mathrm{d}l. \tag{17}$$

Note here, κ and τ are constants for constant radius TSS, and are functions of l for flexible TSS. Take integrations on both sides of Eq. (17), we get the tension transmission for flexible TSS in 3D

$$T_{\tilde{\Phi}} = \begin{cases} T_{in}e^{-\mu\zeta\tilde{\Phi}} - \alpha l\zeta, & \text{if } \tilde{\Phi} < \Phi_0, \\ T_0, & \text{else,} \end{cases} \tag{18}$$

where

$$\tilde{\Phi} = \sum_i \sqrt{\varphi_i^2 + \theta_i^2}, \tag{19}$$

i being each segment of the TSS where κ and τ are constant, Φ_0 as defined in Eq. (12).

In the case of κ and τ both being constant along the TSS, Eq. (19) shrinks to

$$\tilde{\Phi} = \sqrt{\varphi^2 + \theta^2}. \tag{20}$$

An important remark on Eq. (20) is that it only applies when both curvature κ and torsion τ are constant. While being a rather strong condition on the configuration, this is the only condition under which θ and φ can be calculated analytically without the need of segmentation and summation. For general configurations of TSS, even when one of the two variables φ and θ is constant, we cannot obtain a concise formula for $T_{\varphi,\theta}$ like for 2D in Eq. (11).

The discussions on 3D TSS are summarized in Theorem 2.

Theorem 2 (3D). *For a TSS in 3D with terms as defined in Eqs. (1) and (15) and an input tension of T_{in}, the tension at each point along the TSS is given by Eqs. (18) and (19) for general conditions, while Eq. (19) shrinks to Eq. (20) when both κ and τ are constant.*

Theorem 2 suggests that moving from 2D to 3D, the flexibility of changing the configuration of TSS while maintaining the accumulated curve angle, and hence the tension transmission rate, is lost. In 3D TSS, once there is any change in curvature or torsion, the only formula applies would be Eq. (18) with the segmentation and summation. More discussions and validation results will be given in Section 3.

3. Experimental Validation Results

To validate the proposed models, experiments were conducted on a dedicated platform. In this section, after introducing the experimental platform, three experiments will be discussed. We start with the angle effect: tension transmission was measured for a same TSS under different

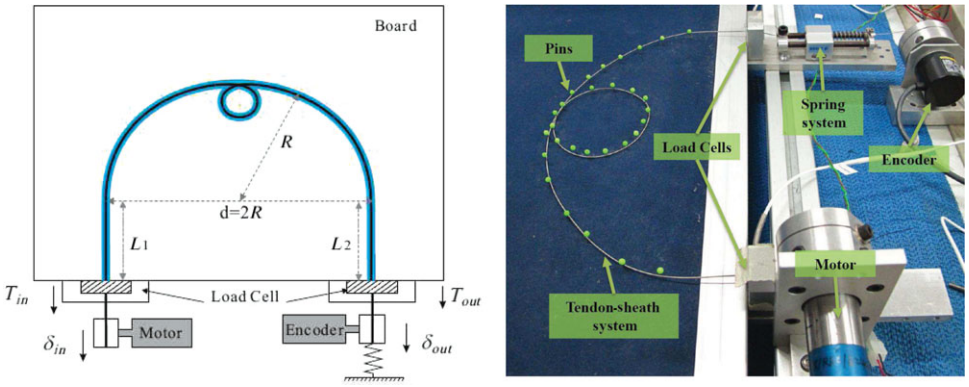

Fig. 3. (Colour online) The experimental platform with a TSS configuration in 2D. On the left is the illustration; on the right is a photo of the real experimental platform.

configurations while maintaining the accumulated curve angle to validate Eq. (11) of Theorem 1. Then, we move on to the length effect: tension transmission of a series of TSS with different lengths but the same bending curve angle was measured to validate Eq. (6) of Proposition 1, as well as its effects on Theorem 1. Finally, the tension transmission of a TSS with configuration in 3D was measured to validate Theorem 2.

3.1. Experimental setup

In order to apply and measure tension to TSS with high level of accuracy and repeatability, a motorized TSS platform was developed. Figure 3 shows the experimental platform. The input side of the tendon is connected to a DC servomotor. The output side of the tendon is attached to a spring and a rotary encoder: the spring ensures that the entire tendon slides inside the sheath (therefore constant ζ); the rotary encoder measures the actual displacement for the output end of the tendon for calculation of elongation. The tendon passes through a flexible wound wire coil used as the sheath. Both ends of the sheath are fixed to the base plates on the same platform, through two washer-type load cells. Thus, during force transmission, the sheath is stopped at the ends against the load cells while the tendon passes through the holes in the middle of the load cells. Hence, the tension in the tendon equals the compression force in the sheath, and is therefore measured by the load cells at both ends. The input and output tendon directions are made parallel to each other, and the distance in between the mounting points is adjustable. A corkboard is used on the platform underneath the sheath, allowing the TSS configuration to be easily restrained by inserting pins on the board.

With the aforementioned platform, the accumulated curve angle could be adjusted by introducing curves or loops along the sheath. Since the beginning and end segment of the TSS are parallel to each other, any convex shape of the TSS in between would have the over curve angle of π. Additionally, each additional full-circle loop to the configuration increases the curve angle by 2π. For instance, the configuration in Fig. 3 has a accumulated curve angle of $\pi + 1 \cdot 2\pi = 3\pi$.

In the experiments, we used Teflon-coated stainless steel 7×7 wire rope of 0.5 mm in diameter as tendon and round wire coil with an outer diameter of 0.9 mm and an inner diameter of 0.6 mm as sheath, both were commercial products for medical applications made by Asahi Intecc, Japan. Encoders were used to record the input and output tendon displacements.

No pretension was applied in the following experiments. Therefore, we always have $T_0 = 0$, hence

$$\Phi_0 = \min\{\varphi \mid T(\varphi) = 0\} = 0. \tag{21}$$

Without pretension, any change of the input tension can reach the output side. However, the actual transmission rate is still governed by transmission laws to be validated.

3.2. The angle effect

In Theorem 1, the curve diameter of the TSS was replaced by the curve angle, as in Eq. (11). We claimed that by making this change, Theorem 1 can be applied to flexible TSS, such that as long as the curve angle remains the same, tension transmission is independent of TSS configuration. To validate this claim, we designed an experiment as follows: a TSS of 1 m in length was mounted to the platform introduced in Section 3.1; the tension transmission rate was measured when the distance between the two ends of the TSS was set to $d = 63.6$ cm; the measurement was repeated with the configuration of the TSS changed to $d = 50$ cm and $d = 70$ cm. In all experiments, only the two ends of the sheath were fixed to the platform, the remaining sheath could move on the platform freely, which resulted in natural convex bending of the TSS, as shown in Fig. 4. For the $d = 50$ cm case, the TSS was constrained from both sides to stop it from extending wider than d, which would violate the convexity assumption.

With a TSS length of 1 m, the TSS forms a half circle when $d = 63.6$ cm, resulting in a curve angle $\varphi = \pi$. Under such configuration, the tension transmission can be calculated using Eq. (4), since the radius of TSS is constant.

For the other two configurations, as d increases and decreases, the TSS no longer forms a perfect half circle. However, due to the mounting mechanism of the platform, the beginning and ending of the TSS were always parallel and perpendicular to the edge of the platform. With the shape of the TSS always convex, the overall curve angle remains π. It is no longer practical to measure TSS radius for calculation at

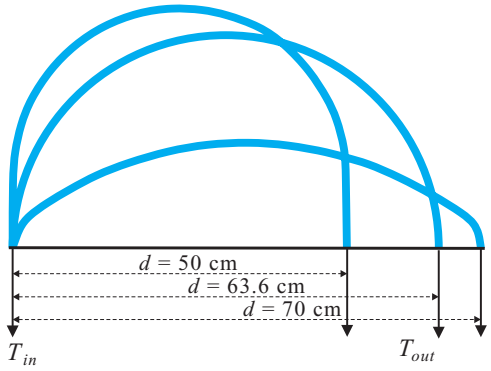

Fig. 4. (Colour online) TSS configurations with d set to 50 cm, 63.6 cm, and 70 cm.

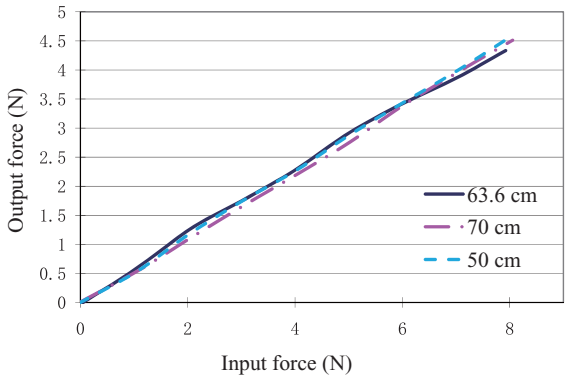

Fig. 5. (Colour online) Experimental results with d set to 50 cm, 63.6 cm, and 70 cm, with the length 1m. While curve path changes, by having the same total curve angle, the transmission ratio remains the same.

each point, therefore Eq. (4) does not apply. However, as long as we know the accumulated curve angle, Theorem 1 applies. Moreover, since the curve angle is not changed, all three experiments should result in the same tension transmission rate.

In the experiment, the motor pulled the tendon at a slow rate of 0.5 mm/s. As the input tension T_{in} increased from 0 to 8 N, the output tension T_{out} was recorded. The results of three different TSS configurations are shown in Fig. 5.

In Fig. 5, the three configurations produced almost identical output tension profiles regardless of the differences in curve diameter. The test was repeated with very similar results except sensor noise variations, hence only one trial of each configuration was shown in the figure.

Next, we verify if Eq. (11) of Theorem 1 catches the essence of tension transmission: the transmission rate T_{out}/T_{in} was measured for a same TSS with 1m in length but with curve angles of $\pi/2$, π, 2π, 3π, and 5π, respectively. The measurement was repeated for three times for each curve angle. We pinned the TSS to the board such that the accumulated curve angle was kept to the desired value of each configuration. However, since the sheath was not fixed to the platform, each time the motor applied tension to the TSS, the sheath would change configuration slightly due to tendon/sheath interactions, hence the actual configuration for each trial would differ slightly even with the same desired accumulated curve angle.

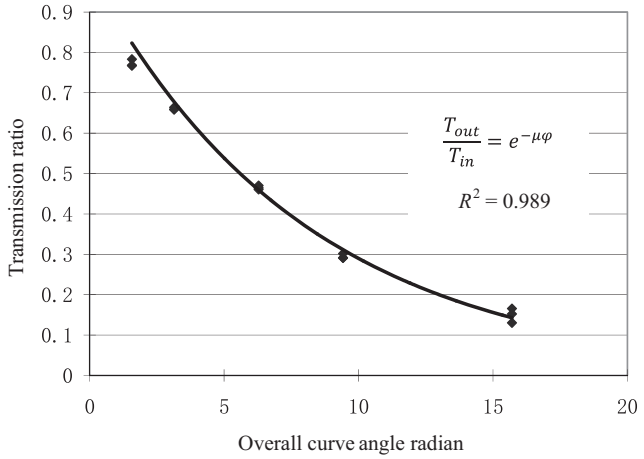

Fig. 6. Experimental results with TSS length of 1m, φ set to $\pi/2$, π, 2π, 3π, and 5π. With TSS length unchanged, tension transmission ratio is an exponential function of the curve angle, with a coefficient of $\mu = 0.124$.

According to Eq. (11), the tension transmission rate should follow an exponential relationship with the curve angle φ. It could be observed in Fig. 6: a very good exponential relationship ($R^2 = 0.989$) between the tension transmission rate and the curve angle. The slight changes in configuration for each trial resulted in minor differences in the three data points, since the TSS was not completely pinned to the board. However, the overall trend for the repeated results validates Eq. (11) overwhelmingly.

There is an interesting and important side product from the results in Fig. 6. The friction coefficient μ can be estimated from the measured data according to Eq. (11), as $\mu = 0.124$. We will compare between different TSS setups in later experiments to see how far can the value obtained from one experiment be generalized.

3.3. The length effect

In Proposition 1 and Eq. (6), we proposed that length has an effect on tension transmission, which was then recalled in the main contributions of Theorems 1 and 2. In this section, we design an experiment to validate this claim, and propose a method to estimate the length effect coefficient α as in Theorems 1 and 2.

The TSS with different lengths was tested for tension transmission. All TSS had a half-circle segment of length 0.3 m in the middle, then completed with two straight lines of equal length that were mounted to the platform. Seven different lengths were tested: 0.3 m, 0.5 m, 0.8 m, 1.1 m, 1.4 m, 1.7 m, and 2 m, respectively. For 0.3 m, the TSS consisted of the half circle only, while for the other lengths the straight line segments increased in length. The configuration setup could be referred to the illustration as shown in Fig. 3. The 2 m configuration had the longest straight-line segments of $L_1 = L_2 = 0.85$ m.

After collecting a series of T_{in} and T_{out} measurements for the TSS of various lengths, there are two ways to obtain α: (1) if the friction coefficient μ is known, Eq. (11) can be used to calculate α; and (2) since the measurements of T_{in} and T_{out} are vectors taken over time, it is possible to estimate both μ

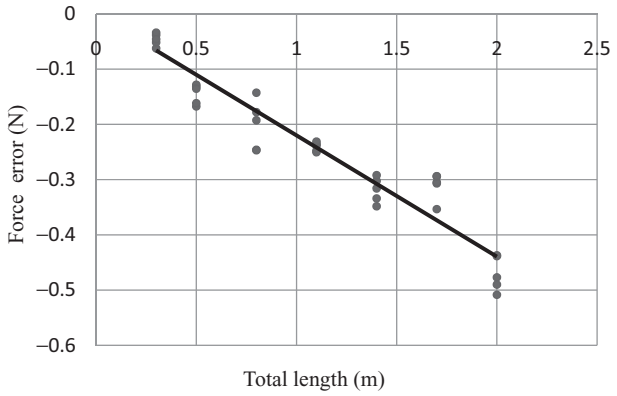

Fig. 7. Results of length effect test with $\bar{e}$ plotted against overall length L of TSS. Each dot represents one test trial. A notable correlation can be observed between length and $\bar{e}$ from the repeated test results.

and α in a least-square sense. Since we did not know if μ estimated from one pair of tendon/sheath can be generalized to another pair and a different piece of tendon/sheath was used in the length test than the angle test, we used method (2) to estimate both coefficients in order to assess the variation of μ between different TSS combinations.

From Eq. (11), we have

$$T_{out} = \begin{bmatrix} e^{-\mu\varphi\zeta} & \alpha \end{bmatrix} \begin{bmatrix} T_{in} \\ -L\zeta \end{bmatrix} \equiv C \cdot X, \tag{22}$$

then a one-step least-square estimation operation was applied to time sequences of T_{out} and X to get an estimation $\hat{C}$. With $\varphi = \pi$ and $\zeta = 1$, we can get estimations $\hat{\mu}$ and $\hat{\alpha}$ of the least-square sense. This procedure was carried out using the 0.3 m length TSS data. As a result, we get

$$\hat{\alpha} = 0.188 \text{ N/m}, \quad \hat{\mu} = 0.097. \tag{23}$$

The new estimated μ value differs significantly (21.7%) from the one obtained from another TSS pair. However, repeating the test five times using the TSS from a same batch, the estimation results show little variation (standard deviation 3.59%). The good repeatability suggests that μ for the tendon/sheath pair for the 0.3 m TSS is different from the one used in the angle test; but on the other hand, it can be generalized to TSS of other lengths, as long as they were taken from the same pair.

Now recall Eq. (4) for fixed radius TSS. As a result of the configuration, each TSS with different length has the same middle segment: a half circle with curve angle of π. The overall length difference was introduced by the straight segments only. Therefore, according to Eq. (4), the tension transmission rate of all TSS with different lengths should be the same. However, as shown in Fig. 7, the time-averaged error $\bar{e}$ between measured T_{out} and calculated T_{out} using Eq. (4) with $\mu = 0.097$, $\varphi = \pi$, and $\zeta = 1$ increases with the overall length of TSS, with an average error $\bar{e}$ defined as

$$\bar{e} = \sum_{j=1}^{N} \frac{\left(T_{out}^{j} - T_{in}^{j}\, e^{-\mu\varphi\zeta}\right)}{N}, \tag{24}$$

where T_{out}^{j} and T_{in}^{j} are the values of T_{out} and T_{in} at time instance j, respectively.

Moreover, the results in Fig. 7 show a linear correlation between $\bar{e}$ and L. Recall Eq. (11) of Theorem 1. Following Eq. (11), e_j is a linear function of L, with sensor noise corrupting T_{out} measurements. With α, L, and ζ being constant values for each given TSS, we get

$$\bar{e} = -\alpha L\zeta + \bar{w}, \tag{25}$$

where $\bar{w}$ is sensor noise. Equation (25) fits well with the experimental results in Fig. 7. In fact, the α value can be estimated for the obtained data as

$$\bar{\alpha} = 0.219\text{N/m}. \tag{26}$$

3.4. Elongation

In this experiment, the elongation model (14) proposed in Theorem 1 is validated. The main difference of Eq. (14), compared to existing results, is the length effect. Since it did not allow flexible configuration for the TSS, here the main focus was placed on the newly proposed length penalty effect on elongation. In tension transmission experiments, we observed that TSS length did have a measurable influence to tension transmission following the propositions. In this experiment, we validate if this can be extended to elongation as well.

Prior to the experiment, a characterization test was carried out first to measure the value of ρ, as introduced in Eq. (14), for the tendon in use. In the characterization experiment, we used a motor to apply tension to the tendon attached to it, and measured the displacement on the tendon as the applied tension increased. As a result, $\rho = 3.16 \times 10^{-4}/N$ and this coefficient is considered to be the same for all tendons with the same material and diameter.

The validation test was then carried out. We measured elongation together with input and output tensions. The curve angle was set to π. Five different TSS lengths were tested: 0.3 m, 0.5 m, 0.8 m, 1.1 m, 1.4 m, 1.7 m, and 2 m, respectively. With the coefficients estimated in the length tests, the elongation values were calculated using Eq. (14) and compared with the measured values.

Two calculations were made for the elongation: one with length effect, the other without. However, for all different lengths, there was no significant difference between the two calculations. The results for the length of 2 m, the longest possible value for the configuration on the experimental platform, are shown in Fig. 8. According to Eq. (14), length effect is larger when the length of TSS is larger; therefore, length effect should be largest for the 2 m TSS in this comparison. As shown in Fig. 8, while both calculation results match with the measured value well, there is hardly

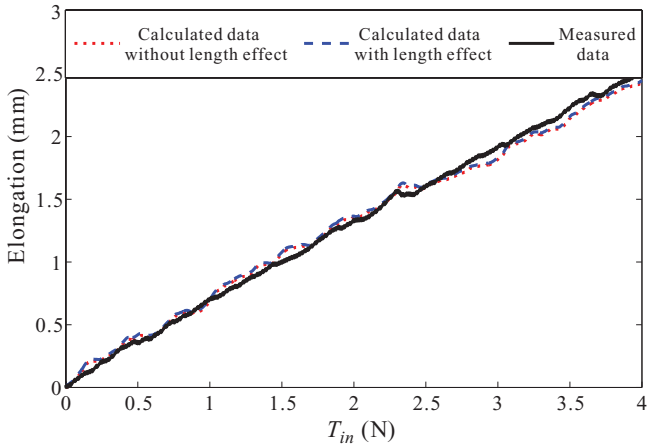

Fig. 8. (Colour online) Results of elongation test with $L = 2$ m. Calculated data fits measured data well. However, length has a much smaller effect to elongation than to tension transmission.

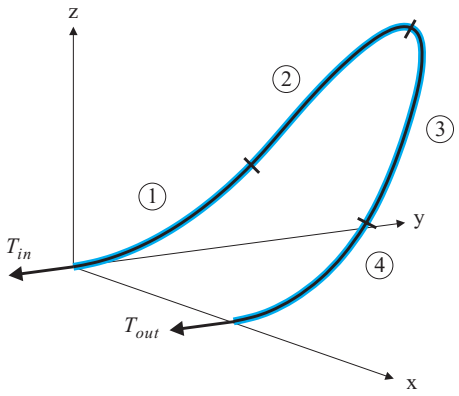

Fig. 9. (Colour online) Configuration of 3D TSS setup.

any separation among themselves. It is noted that the same configuration of 2 m TSS was also tested in the length effect test, the effect of length on the tension was still notable: the elongation in the TSS is much less sensitive to the length effect than the tension.

Such difference should be caused by the multiplication of ρ. Since ρ is a small value (to an order of 10^{-4}), the differences in elongation caused by the length effect were insignificant after multiplied by ρ. Recall that the differences in tension due to length effect as aforementioned were in 10^{-1} N, which could only cause differences in elongation in a magnitude of 10^{-5} m, much smaller compared to the elongation magnitude of 10^{-3} m.

3.5. Tension transmission in 3D

In the end, we validate Theorem 2, where we need to construct a TSS setup in 3D space. Recall Eqs. (18) and (20), curvature and torsion angles follow geometrical summation only when they are equal, although not necessarily constant, at each point. We constructed a TSS setup as shown in Fig. 9. The starting and ending points were in the horizontal plane; curvature κ and torsion τ were equal at each point; no sharp bends throughout the setup; four segments with $\varphi = \pi/4$ and $\theta = \pi/4$ each. The overall length of the 3D TSS was 1 m.

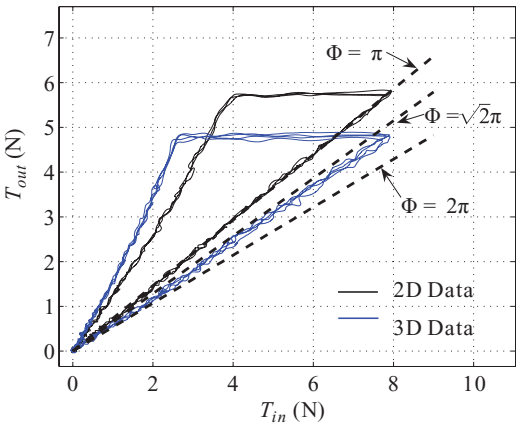

Fig. 10. (Colour online) Results of 3D TSS test.

Measurements of input and output tensions were repeated for five times on the 3D TSS setup. The experimental results are shown in Fig. 10. As a comparison, experimental results of 2D configuration with $L = 1$ m and an accumulated curve angle of π are also plotted.

Here, torsion clearly plays a part in tension transmission: although the accumulated curve angle φ for both the 2D and 3D cases is π, the tension transmission profiles are significantly different with torsion in place in the 3D case than in the 2D case. The difference is repeatable: repeated results clustered well for both 2D and 3D configurations.

Now, the question turns into how to quantify the difference. Following Theorem 2, the equivalent bending angle is given as follows, since $\varphi = \theta$:

$$\Phi = \sum_{j=1}^{4} \sqrt{\varphi_j^2 + \theta_j^2} = \sqrt{2}\pi. \tag{27}$$

Equation (27) suggests that the tension transmission of the 3D configuration should be equivalent to that of a 2D configuration with bending angle of $\sqrt{2}\pi$. To validate this, simulation results of the 2D TSS with length of 1 m and accumulated curve angles of π, $\sqrt{2}\pi$, and 2π are calculated based on the 2D data, and plotted in Fig. 10 in dashed lines. It can be observed that: (1) measured tension transmission profiles of $\Phi = \pi$ match well with the simulated result of $\Phi = \pi$; (2) the measured 3D tension transmission profiles sit between the lines of $\Phi = \pi$ and $\Phi = 2\pi$; and (3) the measured profiles of 3D TSS are close to the simulated profile of $\Phi = \sqrt{2}\pi$ with minor deviations.

The results support our proposed Theorem 2: with curvature and torsion applied at the same time ($\varphi = \pi$, $\theta = \pi$), the resulting tension transmission is equivalent to the 2D configuration with curve angle of the geometry sum of curvature and torsion angles in 3D. There is a noticeable deviation between the measured tension transmission profile of 3D TSS and the simulated profile of $\Phi = \sqrt{2}\pi$. This could result from flexible TSS and the minor changes in the TSS configuration when tension was applied. More discussions on this are given in Section 4.

4. Discussion

The main contributions of this work are summarized in Theorems 1 and 2: the friction model for flexible TSS, the effect of TSS length, and the TSS model in 3D. In this section, we will discuss in depth on the models and the validation experimental results.

4.1. Flexible TSS in 2D

The remedy we proposed to flexible TSS is to use the accumulated curve angle as the integration variable instead of tendon length and curve radius. The idea of using angle instead of tendon length has been mentioned in previous publications, for example, Chen *et al.*[16] But limited by the assumption of fixed radius configuration, instead of aiming at flexible TSS, the angle involved in existing publications was still a continuation of the fixed radius discussion: the arc angle ϕ was used to substitute the ratio of arc length l and the corresponding radius r as in Eq. (4).

Instead of direct variable substitution, we started the analysis from an infinitesimal segment of TSS, and finally proposed a concise and practical way of calculating the tension transmission rate for flexible TSS in Eq. (11) of Theorem 1. Based on the core idea that curve angle being the essential factor for tension transmission, we removed the radius of TSS R from the existing method. This enables the TSS to be *flexible*: as long as the accumulated curve angle is maintained, and the shape of TSS remains convex (φ does not change sign) in a 2D plane, varying the shape of TSS does not affect tension transmission. We also introduced the term *accumulated curve angle*, as a result of solving the integration in Eq. (3), exclusively for flexible TSS as defined in Eq. (10). Validation experiment was carried out as described in Section 3.2, with results showing that changing configuration while maintaining the accumulated curve angle does not change the tension transmission rate.

This change extends the application of the friction model from fixed radius scenarios such as robotic finger actuation and pulley mechanisms to a much broader horizon: tendon-driven mechanisms with complex shapes or even time-varying configurations. Provided that initial calibration is carried out properly, slight changes in TSS configuration can be ignored during operation, as long as they do not violate the two assumptions made above (accumulated angle and convexity).

For elongation, however, the story is different. As in Eq. (14), elongation is a function of the curvature along the tendon, hence affected by the actual TSS configuration. Comparing with the discussion for tension transmission, we can get the following:

Remark 1. Given a TSS of a certain length in a 2D plane, fixed only at both ends, if the TSS configuration changes while preserving (1) accumulated curve angle and (2) convexity, then a same input tension results in a same output tension but potentially a different tendon elongation.

Remark 1 restricts the flexibility of TSS to tension transmission; once fine position control is concerned, TSS configuration cannot be changed without affecting elongation value.

4.2. Length effect

In this paper, we included the effect of TSS length into tension transmission and elongation expressions. This, while addressing the common sense of length-related attenuation of tension, aims at theoretically explaining experimental observations; while meeting practical concerns for applications with very long TSS (compared with its own diameter). We proposed the length effect coefficient α to model the length effect. It was proven in the experiment that α is a characteristics of a particular tendon and sheath pair.

In view of comparing TSS of different diameters, a tendon with a smaller diameter was used in a preliminary experiment. In the results, the length effect was not measurable with the utilized sensing devices. Although we believe that given TSS long enough, the accumulated tension attenuation due to length effect would be measurable, it would fall beyond the constraint of our experimental platform. As no presentable difference was observed, the results of the preliminary experiment were not shown here. We then switched to the current tendon with larger diameter (sheath is kept the same) and as shown in the results, the length effect became measurable within the practical range of our platform. Despite that, the overall length effect to tension transmission for the current tendon-sheath pair is still small comparing to the bending angle effect. For $L = 2\,\mathrm{m}$, the accumulated tension attenuation due to length effect was merely $0.5\,N$, barely above the noise level of the load cell in use. Here, we make the following two remarks on length effect:

Remark 2. α is related to the tendon/sheath pair. The larger the tendon diameter, the smaller the sheath diameter, the larger value of α. Therefore, to minimize length effect, the selection of driving tendon shall be as thin as possible while the sheath having preferably a larger inner diameter.

Remark 3. α is different from μ. α has a unit of N/m while μ being unit-less. Since in our experiment, there was a diameter margin between tendon/sheath, the length effect is not friction due to encirculation. Therefore, α is different from μ.

For elongation, again, the story is different. As shown in the validation experiment results, even with the thickest available tendon that can fit to the sheath in use and the longest possible TSS for the platform, the elongation length effect was still not measurable. The value of ρ plays an important roll here: it shrinks the length effect by an order of 10^{-2} to 10^{-4} depending on the tendon in use. By definition of ρ as $1/EA$, the stiffer the material, the larger the section area, the smaller the ρ value, hence the smaller the length effect on elongation.

Remark 4. To minimize the length effect to elongation, three factors should be considered: (1) diameter margin between tendon and sheath is preferably large; (2) tendon diameter/section area is preferably large; and (3) tendon material is preferably stiff with a high Young's module E.

In application, the TSS diameter is usually limited by the size of the working channel, hence the diameter of neither the tendon nor the sheath could be large. Therefore, a

material with high Young's module would be preferable, and a compromise must be made between the tendon diameter and the margin left in between.

4.3. TSS in 3D

It is inevitable that flexible TSS gets placed in a 3D space. However, the results of this paper suggest that there is a price in doing so. With torsion coming into play, the freedom of TSS flexibility in 2D is lost: the profile of torsion and curve angles will now affect the overall tension transmission.

In the validation results, we only fixed the TSS at certain turning points. When the input tension is applied, the TSS will flex as the tension increases, resulting in a slight change in configuration. As a result, there is a noticeable deviation between measured 3D data and simulated data of $\Phi = \sqrt{2}\pi$. Here, a remark is made on how to place a TSS in 3D configuration to get maximum tension transmission.

Remark 5. For a TSS of 3D configuration, the highest tension transmission rate can be achieved only when the curvature and torsion are equal at all points.

Recall Eq. (18), we have

$$\bar{\Phi} = \sum_i \sqrt{\varphi_i^2 + \theta_i^2} \geq \sum_i \sqrt{2\varphi_i\theta_i}, \tag{28}$$

therefore, $\bar{\Phi}$ only reaches its minimum (where tension transmission is at its maximum, see Theorem 2) when $\varphi_i = \theta_i$ for all i. Remark 5 suggests that if a TSS is to be place in 3D space with known input and output angles, the optimal configuration in terms of maximizing tension transmission would be to keep curvature and torsion the same at all times.

Although the formula to calculate the tension transmission rate in 3D configuration has been validated by experiment, the formula itself becomes impractical: we need to know each and every value of curve angle φ and torsion angle θ to calculate output tension, which means fixing the entire TSS.

However, using segmentation of the TSS, we can still divide each TSS into 2D segments and 3D ones. A remedy is proposed here.

Remark 6. Free-flexing of TSS can only be allowed in 2D planes. If a TSS needs to be placed in 3D configuration, it should be divided into several segments: the ones with 3D configurations should be fixed; only the ones in 2D planes can change in configuration within the constraints introduced in Remark 1.

Remark 6 provides a practical remedy for TSS that needs to pass through 3D space. If, with specifically designed supporting mechanisms, the flexible segments of the TSS can be restricted within 2D planes and the 3D segments have controllable/measurable curve diameters, the overall tension transmission could be measured and even maintained when the 2D segments are flexible.

5. Conclusions

We proposed three main contributions to tension transmission and elongation for TSS analysis. First, the length penalty effect was studied and a linear simplified model was proposed in Proposition 1 to approximate the effect, such that the additional tendon tension loss follows a linear relationship with the length of TSS. Guidelines in how to minimize the length effect were given in the discussion section. Then, we proposed a tension transmission model for 2D TSS in Theorem 1, incorporating the length effect, that allows for flexible TSS configurations. It is worth noting that the proposed model is applicable for the TSS with fixed radii as well. This model allows the configuration of TSS to be changed within certain boundaries without affecting the tension transmission rate. Elongation was also studied. Although the flexibility in tension transmission cannot be generalized to elongation, we discussed the sensitivity of elongation to the length effect and gave guidelines to minimize the effect. In the end, the discussion was extended to 3D configuration of the TSS, with a model proposed in Theorem 2. The model shows that flexibility is not possible for general 3D configurations, but a remedy was given in Remark 6 on how to apply 3D TSS to obtain flexibility.

The study paves the way to remote mechanical actuation of robotic devices. Disregard of the space limitations, sufficient actuation energy could be generated from the outside actuation source and transferred via the TSS to the distal end through a narrow working channel. The crucial point is, we need to know accurately the transfer function of the TSS. With the proposed models, tension transmission in 2D, and even in 3D with remedies, could be easily modeled by measuring or calculating the accumulated curve angle. The length effect is an important proposition for applications with very long and narrow tunnels: although for general applications this effect is negligible, it is needed for the extreme cases to make accurate modeling possible.

A direct application of this study is robotic endoscopy.[24] An endoscope is a typical example of a long and narrow working channel that could change its configuration in 3D space constantly as it navigates through the gastrointestinal tract of a human body.[25] Feasibility of the endoscopic robots adopting TSS as power transmission has been tested in clinical surgical tasks.[26,27] The proposed models, as well as the refined ones in future work, will hopefully be applied to introduce haptic feedback and precise control to the endoscopic surgical robot.

Acknowledgment

The research was supported by the Translational Clinical Research (TCR) grants NMRC/TCR/001-NUS/2007, from the National Medical Research Council (NMRC) of Singapore.

References

1. A. Wolf, H. B. Brown, R. Casciola, A. Costa, M. Schwerin, E. Shamas and H. Choset, "A Mobile Hyper Redundant Mechanism for Search and Rescue Tasks," *International Conference on Intelligent Robots and Systems*, Las Vegas, USA (2003) pp. 2889–2895.
2. A. Ahrary, A. A. F. Nassiraei and M. Ishikawa, "A study of an autonomous mobile robot for a sewer inspection system," *Artif. Life Robot.* **11**(1), 23–27 (2007).

3. S. J. Phee, A. P. Kencana, V. A. Huynh, Z. L. Sun, S. C. Low, K. Yang, D. Lomanto and K. Y. Ho, "Design of a master and slave transluminal endoscopic robot for natural orifice transluminal endoscopic surgery," *Proc. Inst. Mech. Eng.* **224**(7), 1495–1503 (2010).
4. K. Harada, D. Oetomo, E. Susilo, A. Menciassi, D. Daney, J.-P. Merlet and P. Dario, "A reconfigurable modular robotic endoluminal surgical system: vision and preliminary results," *Robotica* **28**(2), 171–183 (2010).
5. M. Rasouli and S. J. Phee, "Energy sources and their development for application in medical devices," *Expert Rev. Med. Devices* **7**(5), 693–709 (2010).
6. K. H. Low, *Mechanics of Mechanisms: Basic and Systematic Approaches*, 3rd ed. (Prentice Hall, Singapore, 2006).
7. R. J. Webster III, A. M. Okamura and N. J. Cowan, "Toward Active Cannulas: Miniature Snake-Like Surgical Robots," *International Conference on Intelligent Robots and Systems*, Beijing, China (2006) pp. 2857–2863.
8. N. Simaan, K. Xu, W. Wei, A. Kapoor, P. Kazanzides, P. Flint and R. Taylor, "Design and integration of a telerobotic system for minimally invasive surgery of the throat," *Int. J. Robot. Res.* **28**(9), 1134–1153 (2009).
9. R. J. Webster III and B. A. Jones, "Design and kinematic modeling of constant curvature continuum robots: A review," *Int. J. Robot. Res.* **29**(13), 1661–1683 (2010).
10. Z. Sun, R. Y. Ang, E. W. Lim, Z. Wang, K. Y. Ho and S. J. Phee, "Enhancement of a master-slave robotic system for natural orifice transluminal endoscopic surgery," *Ann. Acad. Med. Singap.* **40**(5), 223–230 (2011).
11. J. J. Lee and L. W. Tsai, "The structural synthesis of tendon-driven manipulators having a pseudotriangular structure matrix," *Int. J. Robot. Res.* **10**(3), 255–262 (1991).
12. H. Kobayashi, K. Hyodo and D. Ogane, "On tendon-driven robotic mechanisms with redundant tendons," *Int. J. Robot. Res.* **17**(5), 561–571 (1998).
13. M. Kaneko, T. Yamashita and K. Tanie, "Basic Considerations on Transmission Characteristics for Tendon Driven Robots," *International Conference on Advanced Robotics*, Pisa, Italy (1991) pp. 827–832.
14. G. Palli and C. Melchiorri, "Model and Control of Tendon-Sheath Transmission Systems," *International Conference on Robotics and Automation*, Orlando, USA (2006) pp. 988–993.
15. F. Tian and X. Wang, "The Design of a Tendon-Sheath-Driven Robot," *International Conference on Mechatronics and Machine Vision in Practice*, Auckland, New Zealand (2008) pp. 280–284.
16. L. Chen, X. Wang and F. Tian, "Tendon-Sheath Actuated Robots and Transmission System," *International Conference on Mechatronics and Automation*, Changchun, China (2009) pp. 3173–3178.
17. V. Agrawal, W. J. Peine and B. Yao, "Modeling of transmission characteristics across a cable-conduit system," *IEEE Trans. Robot.* **26**(5), 914–924 (2010).
18. Z. Wang, J. Hoelldampf and M. Buss, "Design and Performance of a Haptic Data Acquisition Glove," *Proceedings of the 10th Annual International Workshop on Presence*, Barcelona, Spain (2007) pp. 349–357.
19. Z. Wang, A. Peer and M. Buss, "Fast Online Impedance Estimation for Robot Control," *IEEE International Conference on Mechatronics*, Malaga, Spain (2009) art. 4957217.
20. Z. Wang, *High-Fidelity Haptics in Multimodal Human-Robot Interaction*, 1st ed. (VDI-Verl, Germany 2010).
21. S. C. Low, S. J. Phee, P. Valdastri, A. Menciassi and P. Dario, "Tendon Sheath Analysis for Estimation of Distal End Force and Elongation," *International Conference on Advanced Intelligent Mechatronics*, Singapore (2009) pp. 332–337.
22. S. J. Phee, S. C. Low, P. Dario and A. Menciassi, "Tendon Sheath Analysis for Estimation of Distal End Force and Elongation for Sensorless Distal End" *Robotica* **28**(7), 1073–1082 (2010).
23. J. L. Pons, R. Ceres and F. Pfeiffer, "Multifingered dextrous robotics hand design and control: A review," *Robotica* **17**(6), 661–674 (1999).
24. Z. Wang, Z. Sun and S. J. Phee, "Haptic feedback and control of a flexible surgical endoscopic robot," *Computer Methods and Programs in Biomedicine*, doi:10.1016/j.cmpb.2013.01.018 (Apr. 2, 2013).
25. S. J. Phee, Z. Sun, Z. Wang, J. Y. Y. Wong and K. Y. Ho, "The future of transluminal surgery," *Expert Rev. Med. Devices* **8**(6), 669–671 (2011).
26. Z. Wang, S. J. Phee, D. Lomanto, R. Goel, P. Rebala, Z. L. Sun, S. Trasti, N. Reddy, J. Y. Y. Wong and K. Y. Ho, "Endoscopic submucosal dissection of gastric lesions by using a master and slave transluminal endoscopic robot: An animal survival study," *Endoscopy* **44**(7), 690–694 (2012).
27. S. J. Phee, N. Reddy, P. W. Y. Chiu, R. Pradeep, G. V. Rao, Z. Wang, Z. L. Sun, J. Y. Y. Wong and K. Y. Ho, "Robot-assisted endoscopic submucosal dissection is effective in treating patients with early-stage gastric neoplasia," *Clin. Gastroenterol. Hepatol.* **10**(10), 1117–1121 (2012).